

CTI HISTORY OF THE EPIC PN CAMERA

K. Dennerl, U.G. Briel, M.J. Freyberg, F. Haberl, N. Meidinger, and V.E. Zavlin

Max-Planck-Institut für extraterrestrische Physik, Giessenbachstraße 1, 85748 Garching, Germany

ABSTRACT

The pn camera of EPIC is inherently robust against radiation damage effects. Nevertheless, the knowledge of charge transfer inefficiency (CTI) of the pn camera is crucial for obtaining the correct energy scale. We describe detailed in-orbit monitoring of this effect, utilizing the internal calibration source. We find that during the first two years in orbit the CTI increased by $\sim 4\%$ for Al- K_α and by $\sim 7\%$ for Mn- K_α . The increases in the CTI are well within expectations, with no measurable effect on the energy resolution.

Key words: Missions: XMM-Newton – EPIC pn – energy calibration – charge transfer inefficiency (CTI) – radiation damage

1. INTRODUCTION

In CCDs electrons of the signal charge generated by an absorbed X-ray photon are lost during transfer to the readout node by traps in the transfer channel. The number of traps is expected to increase with time due to radiation damage. As the knowledge of the charge loss is essential for extracting quantitative spectral information, the performance of the EPIC pn camera is routinely monitored with an internal calibration source. This source consists of radioactive Fe^{55} with an Al-target, and irradiates the detector with Al- K_α and Mn- K_α emission lines at 1.5 and 5.9 keV. This is usually done for about one hour at the beginning of each 48 hour revolution of XMM-Newton. The line positions determined from these exposures are a sensitive indicator for any change in the energy response.

2. GROUND CALIBRATION

The importance of the CTI for the energy calibration of the EPIC pn camera was realized long before launch, and a lot of experience was gained during extensive laboratory measurements with different detectors at different temperatures and energies. We developed specific software tools for the CTI analysis of such calibration data, which allow us to determine the charge loss across the 768 readout channels with high spatial resolution. Fig. 1 illustrates the method. Results from laboratory measurements for the

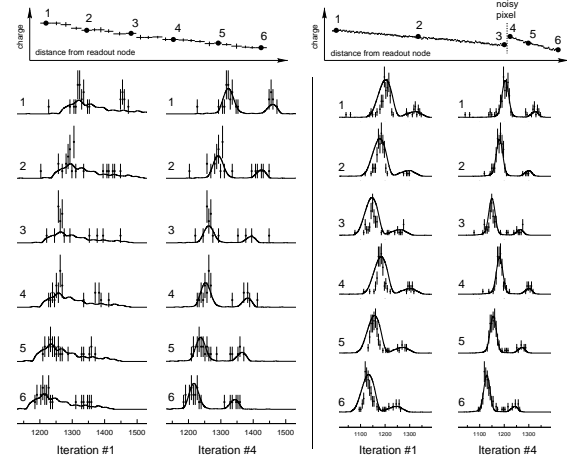


Figure 1. Illustration of the charge loss determination by the template cross correlation method, for the case of low (left) and high (right) statistical quality. In both cases the two columns show the results of template fits to spectra from selected macro pixels for the first (left) and last (right) iteration. The macro pixels are identified by filled circles in the resultant charge loss curves at top, where the apparent energy of the emission line is plotted against the distance from the readout node. In the case at left only 631 events were recorded within the whole CCD column, leaving only 20–29 events for each of the 25 macro pixels. At right, 17864 events were available in total, sufficient for applying this technique to each individual pixel. Note how significantly the presence of a noisy pixel reduces the charge loss for events which were shifted across this pixel during readout. In both cases Mn- K_α and K_β lines were analysed.

detector now onboard XMM-Newton are shown in Figs. 2 and 3. More about the energy calibration before launch can be found in Dennerl et al. (1999). Here we report on recent results obtained from monitoring the CTI in orbit.

3. CTI MONITORING IN ORBIT

The number of photons obtained during the ~ 1 hour calibration measurements in orbit is not sufficient for the determination of the charge loss for individual columns. However, during six revolutions (# 23, 80, 125, 172, 242, and 332) long measurements were made with exposures of

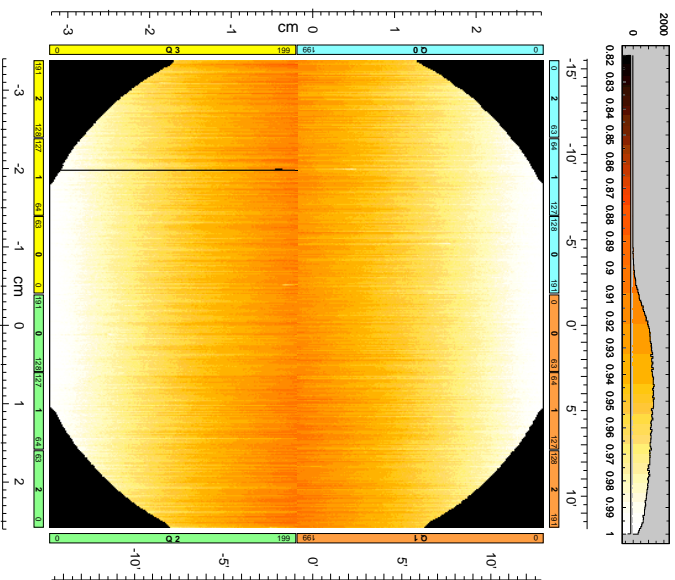


Figure 2. Residual charge map at Fe-K_α , derived from a superposition of several long flatfield exposures during ground calibration at Orsay, where more than 80 million events were recorded. The colour of each pixel indicates the fraction of the charge which arrives at the readout node, in the colour coding which is displayed at top together with a frequency histogram. Charge losses of up to 10% occur, and by this amount the Fe-K_α line energy would shift across the detector, if no CTI correction were applied.

13 up to 21 hours duration, where the statistical quality is comparable to laboratory measurements. Fig. 4 shows the charge losses determined from rev.125, and Fig. 7 in Briel et al. (2002, these proceedings) summarizes the CTI history for CCDs 1, 2, and 3 (quadrant 0), derived from the six measurements.

In order to extend the CTI analysis to the shorter exposures, we modified our technique in the following way: we combined events, with the same distance from the readout node, from several readout columns, after having corrected their raw amplitudes for the gain of the particular column. As the irradiation is not homogeneous across the detector (Figs. 5 and 6), we selected only events from the better exposed areas, which are less contaminated by out-of-time events. The spectra of such ‘macro columns’ were then analysed in the same way as those of individual columns (cf. Fig. 1). Fig. 7 illustrates the accuracy which can be reached with this method.

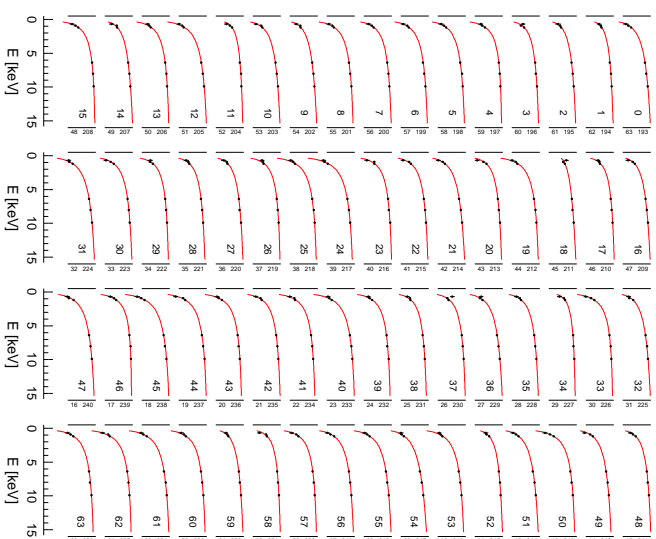


Figure 3. Energy dependence of the CTE ($= 1.0 - \text{CTI}$) for all columns of CCD 4, as measured before launch. Dots indicate the measurements, while the solid lines were obtained by fitting the measurements with the function $\text{CTE}(E) = a_0 + a_1 \log E + a_2 (\log E)^2$ to the observed values. Vertical lines along the CTE curves cover the range from 0.9990 to 0.9997 in a linear scale.

4. RESULTS

Fig. 8 summarizes the CTI results for Al-K_α and Mn-K_α obtained for quadrant 0, which receives relatively homogeneous irradiation (Figs. 5, 6). We find the CTI at Al-K_α and Mn-K_α to increase slowly with time, with a rate of $\sim 1.5 \cdot 10^{-5} \text{ yr}^{-1}$ for both energies.

This is in contrast to the considerable scatter seen in the Mn-K_α line positions, which result when we apply the same CTI correction to the calibration data (Fig. 9). We found that the short-term drops of the line position were not caused by CTI changes, but by changes in the amplification, which were the consequence of temperature variations in the electronic boxes. The drops in the line position show a clear correlation with the temperature and can thus be well corrected. Short-term rises of the line position, on the other hand, were found to be correlated with periods when the background radiation was so high that no astrophysical observations could be performed. Despite all the scatter, however, Fig. 9 shows evidence for a long-term decrease of the line position, which is indeed caused by the increase of the CTI.

How does the CTI increase seen during the first two years in space compare with pre-launch predictions? For



Figure 4. Charge loss and CTE for individual columns of quadrant 2 at Mn- K_α , obtained from a 18 hour exposure with the internal calibration source during revolution 125. The high statistical quality made it possible to determine the charge losses for individual pixels. The curves show the apparent line energy as a function of the distance from the readout node. When shifted along the whole column, the charge losses accumulate to $\sim 10\%$. The first number at the curves identifies the column, while the second number gives the CTE in the form $(CTE - 0.999) \cdot 10^5$, i.e. the last two digits xx of $0.999xx$. The CTE was obtained by fitting an exponential function to the charge losses. At bottom the CTE values of all columns are summarized. Significant differences between the individual columns are obvious. The shaded region shows the standard deviation of the CTE values, which is printed to the right together with the mean value.

Mn- K_α we measure a long-term trend of

$$\frac{dCTI}{dt} = +(1.5 \pm 0.1) \cdot 10^{-5} \text{ yr}^{-1}.$$

Before launch, laboratory measurements, taken at -90° C , the operating temperature of the EPIC pn camera in orbit, showed the following response of the CTI to a 10 MeV proton equivalent flux F_{rad} for Mn- K_α (Meidinger et al. 1998):

$$\frac{dCTI}{dt} = 4 \cdot 10^{-13} \text{ cm}^2 \cdot F_{\text{rad}}$$

For F_{rad} , an average value of $5 \cdot 10^7 \text{ cm}^{-2} \text{ yr}^{-1}$ was expected, yielding

$$\frac{dCTI}{dt} = +2 \cdot 10^{-5} \text{ yr}^{-1}$$

at Mn- K_α . Thus, the measured value is even somewhat lower than this estimate.

The additional noise created by the small relative increase of the CTI is almost negligible and should not have measurable consequences for the energy resolution. In fact, no significant increase of the width of the Mn- K_α line was observed over the first two years (Fig. 10).

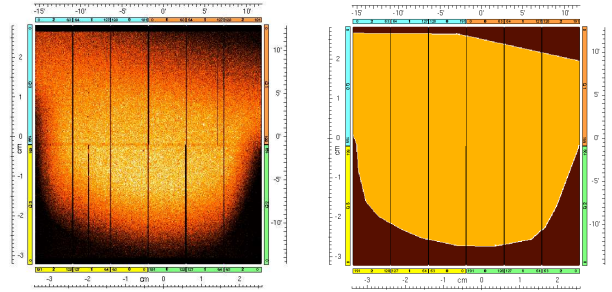


Figure 5. Irradiation at Al- K_α and corresponding mask.

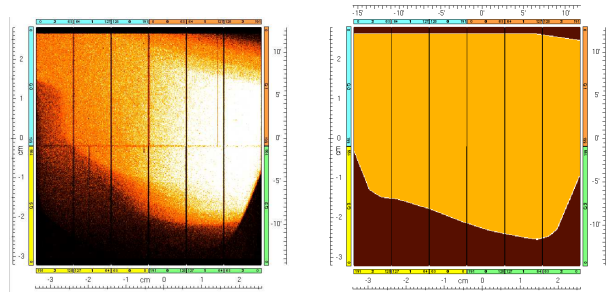


Figure 6. Irradiation at Mn- K_α and corresponding mask.

5. SUMMARY AND CONCLUSIONS

From routine measurements with the internal calibration source, the CTI of the EPIC pn camera was found to increase by $+(1.4 \pm 0.4) \cdot 10^{-5} \text{ yr}^{-1}$ at Al- K_α ,

and by $+(1.5 \pm 0.1) \cdot 10^{-5} \text{ yr}^{-1}$ at Mn- K_α .

This corresponds to a relative increase of the CTI by $\sim 4\%$ for Al- K_α and by $\sim 7\%$ for Mn- K_α during the first two years in orbit, with no measurable effect on the energy resolution. If this trend continued, then it would take more than 25 years until the CTI at Mn- K_α would have doubled. At Al- K_α , the CTI would then have increased by about half of its present value.

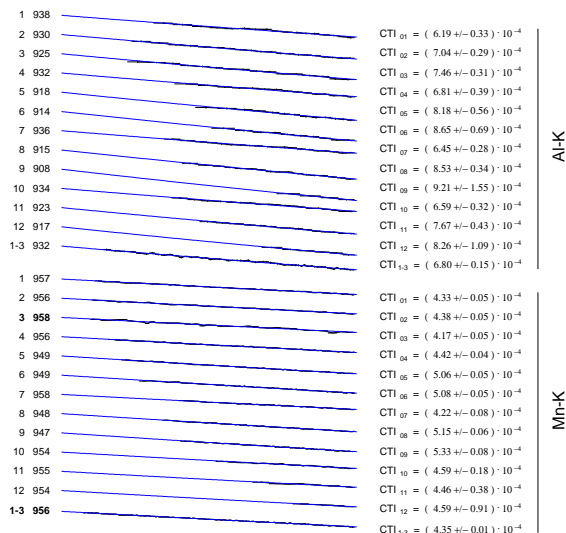


Figure 7. Charge loss and CTI for individual CCDs, and for quadrant 0. This plot is similar to Fig. 4. Here, however, photons from several columns were combined (after having been corrected for individual gain variations), to increase the statistical quality and to extend the CTI analysis to shorter exposures. The data were taken from a 2 hour exposure with the internal calibration source during revolution 285. The curves refer to CCDs 1–12, and to quadrant 0, for Al– K_{α} (top) and Mn– K_{α} (bottom). Gaps are caused by poorly exposed regions (cf. Fig. 5, 6). The CTI values, determined from exponential fits, are listed to the right of each curve.

ACKNOWLEDGEMENTS

The XMM–Newton project is an ESA Science Mission with instruments and contributions directly funded by ESA Member States and the USA (NASA). The XMM–Newton project is supported by the Bundesministerium für Luft- und Raumfahrt (BMBF /DLR), the Max–Planck–Gesellschaft and the Heidenhain–Stiftung.

REFERENCES

- Briel, U.G., Dennerl, K., Freyberg, M.J., et al. 2002, these proceedings
 Dennerl, K., Briel, U.G., Haberl, F., et al. 1999, SPIE, 3765, 232
 Meidinger, N., Schmalhofer, B., Strüder, L., 1998, IEEE Trans. on Nucl. Sci, 45, 2849

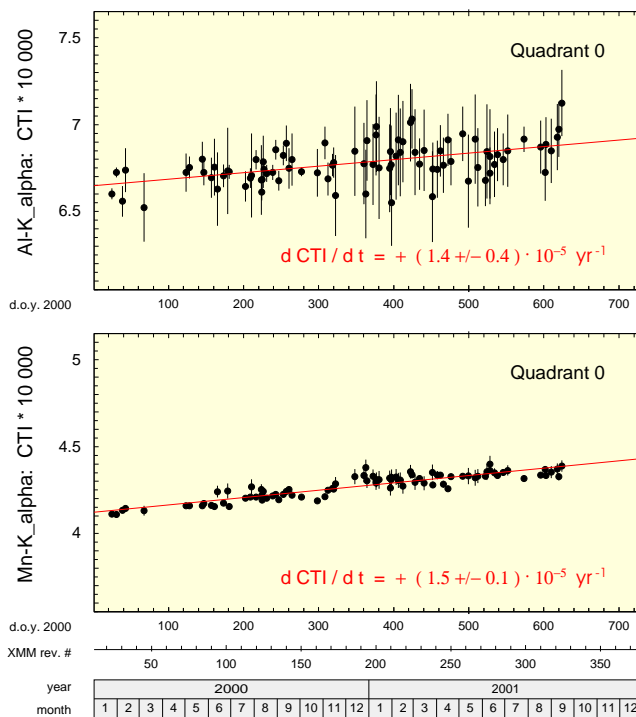


Figure 8. Results of the CTI determination from internal calibration measurements in orbit, for quadrant 0 at Al– K_{α} (top) and Mn– K_{α} (bottom). Both energies show a consistent slope, which is significantly different from zero in both cases.

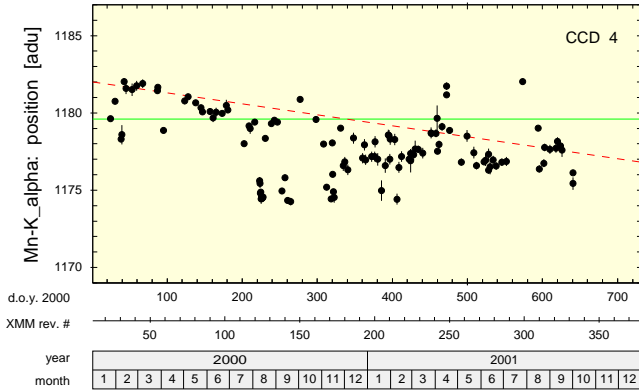


Figure 9. $Mn-K_{\alpha}$ line position, not corrected for CTI history. In the first months after the launch of XMM-Newton, short-term drops of the peak position on time scale of days showed up, caused by temperature variations in the electronic boxes, while brief, sudden rises were found to be related to episodes of very high background. In addition to these short-term changes there are indications for a long-term decrease of the line position (dashed red line), which is caused by a CTI increase. The green line marks the nominal value of $Mn-K_{\alpha}$ for an amplification of 5 eV/adu.

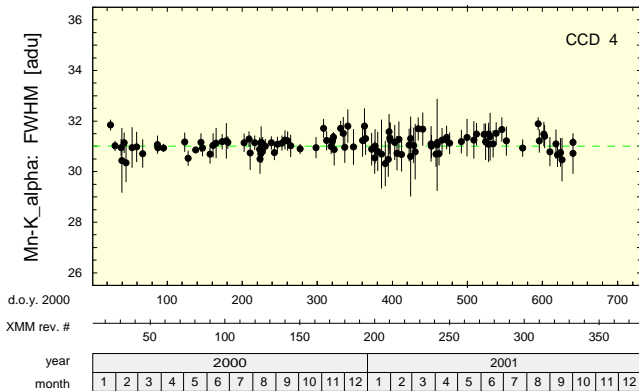


Figure 10. Energy resolution for $Mn-K_{\alpha}$. The FWHM of 31 adu corresponds to 155 eV. During the first two years in orbit, no change in the energy resolution was observed.